Tectonophysics, 192 (1991) 367–382
Elsevier Science Publishers B.V., Amsterdam

A two-dimensional interpretation of the geomagnetic coast effect of southeast Australia, observed on land and seafloor

R.L. Kellett [a,1], F.E.M. Lilley [a] and A. White [b]

[a] *Research School of Earth Sciences, Australian National University, Canberra, A.C.T. 2601, Australia*
[b] *School of Earth Sciences, Flinders University of South Australia, Bedford Park, S.A. 5042, Australia*

(Received May 4, 1990; accepted November 22, 1990)

ABSTRACT

Kellett, R.L., Lilley, F.E.M. and White, A., 1991. A two-dimensional interpretation of the geomagnetic coast effect of southeast Australia, observed on land and seafloor. *Tectonophysics*, 192: 367–382.

Data from detailed investigations of the geomagnetic coast effect across the southeast Australian continental margin are interpreted in terms of a two-dimensional numerical model. There is both land and seafloor control on this model, and both *E*-pol and *B*-pol mode responses are incorporated.

The good fit to the data of a model comprising ocean water and marine sediments is improved when the sub-ocean electrical conductivity profile is allowed to differ from the continental conductivity profile. A final model is determined by an inversion procedure based on systematic search. The main characteristic of this model is that an increase in conductivity occurs at a shallower depth beneath the ocean than beneath the land (some 100 km beneath ocean, 200 km beneath land).

The southeast continental margin of Australia is considered to have formed by passive rifting, at the time of the opening of the Tasman Sea. A depth of 100 km for the base of the oceanic lithosphere corresponds well to the age of rifting some 80 Ma ago. The contrast with the continental profile suggests an electrical asthenosphere relatively deeper beneath southeast Australia.

1. Introduction

Near many coastlines, a strong correlation occurs between the vertical and horizontal components of the fluctuating magnetic field. First studied by Parkinson (1959), the phenomenon is commonly known as the geomagnetic coast effect. It is the subject of many papers, for example Everett and Hyndman (1967), Parkinson and Jones (1979), White and Polatajko (1978), and Neumann and Hermance (1985). Initially observations were restricted to those made on land, but subsequently observations on the ocean side of coastlines have become possible, with the development of instruments for measuring seafloor magnetic and electric fields (Filloux, 1988).

The ocean water itself, being highly electrically conducting, is clearly a major contributor to the geomagnetic coast effect. A point of long-standing interest is what other electrical conductivity structure, in the crust and upper mantle, may be necessary at a continent–ocean boundary to explain the phenomenon.

The present paper contributes to the study of the coast effect at passive (i.e. Atlantic-type) continental margins. In particular the present paper forms a sequel to White et al. (1990) and other earlier papers regarding the coast effect of southeast Australia. White et al. (1990) added the marine observations of the 1986 Continental Slope Experiment (CSE) to the land and deep seafloor observations of the 1983/84 Tasman Project of Seafloor Magnetotelluric Exploration (hereafter referred to as the "Tasman Experiment"), to give a complete traverse of observing sites from inland Australia to the deep seafloor.

[1] Département de Génie Mineral, Ecole polytechnique, Montreal, Que., H3C 3A7, Canada.

0040-1951/91/$03.50

The coastline of southeast Australia extends for some 500 km in a straight line, without major bays or promontories, on either side of the Tasman Experiment profile; it is thus an ideal coastline for two-dimensional modelling. While there is some evidence (Ferguson, 1988; Lilley et al., 1989; Ferguson et al., 1990) for three dimensional effects in the marine observations, (which a numerical thin-sheet model for the whole Tasman Sea is presently being constructed to investigate—Heinson and Lilley, 1989), the sites used in the present paper are positioned most effectively to make the two-dimensional approximation valid. The location of the coastline beneath the uniform mid-latitude source fields additionally makes southeast Australia a particularly suitable region for investigating the geomagnetic coast effect.

The observations from both the Tasman Experiment and the Continental Slope Experiment are presented below using the hypothetical event analysis technique of Bailey et al. (1974), and the time-series analysis used to produce the transfer functions assumes a time dependence of $e^{-i\omega t}$. The observations cover a period range from 600 s to 200,000 s and many of the time-series, in particular the marine data, contain strong signals at the known frequencies of the ocean tides. While such tidal signals are of great interest on their own account (see, for example, Bindoff, 1988, and Bindoff et al., 1988) they have been removed in the present analysis by filtering.

The marine and land data have been analysed in an identical manner. However, it should be remembered throughout this paper that for both observation and model response, land data are given for the land–air interface, whilst marine data are given for the seafloor-seawater interface. Care must be exercised when interpreting parameters such as Parkinson arrows across both environments.

2. Sources of data

The sources of data are basically the Tasman and Continental Slope Experiments which, together, occupied the recording sites shown in Fig. 1. For the Tasman Experiment, much of the data reduction is the work of Ferguson (1988), and the seafloor magnetotelluric impedances used in the present paper have been taken from that source. Ferguson et al. (1990) use the impedances from the central Tasman Sea in a one-dimensional analysis of the deep conductivity structure. Details of the Continental Slope Experiment are given in Kellett et al. (1988), White et al. (1990) and Kellett (1989). Some of the land instrument sites lie close to observation points occupied in the previous studies of Everett and Hyndman (1967), Tam-

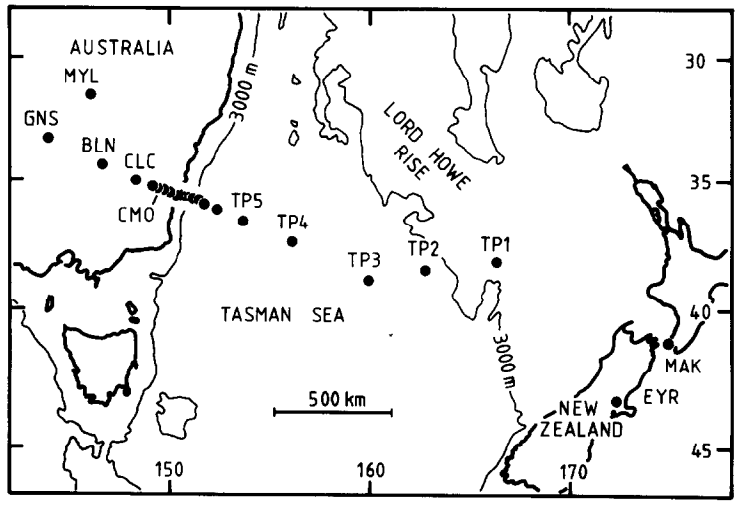

Fig. 1. A map of the Tasman Sea region showing the observation sites for the Tasman and Continental Slope Experiments.

memagi and Lilley (1971), and Bennett and Lilley (1971), and the present data set has been checked for consistency with the results of the earlier studies.

3. Induction arrows

3.1 Computation

Analysis has been carried out on the magnetic fluctuation data to produce both vertical field and horizontal field "induction arrows". These arrows are shown in Fig. 2, for a period band centred on 7484 s.

Each set of arrows has been computed taking as the "normal" or reference site the westernmost station GNS. This site is chosen because of its greatest distance inland from the coast, and thus for its direct correspondence with the regional field of the modelling program. The arrows are thus slightly different from those of Ferguson (1988) and Lilley et al. (1989), which were based on Canberra Magnetic Observatory (CMO) as reference, and to produce the former from the latter the computation of further inter-station transfer functions has been necessary (Banks 1986).

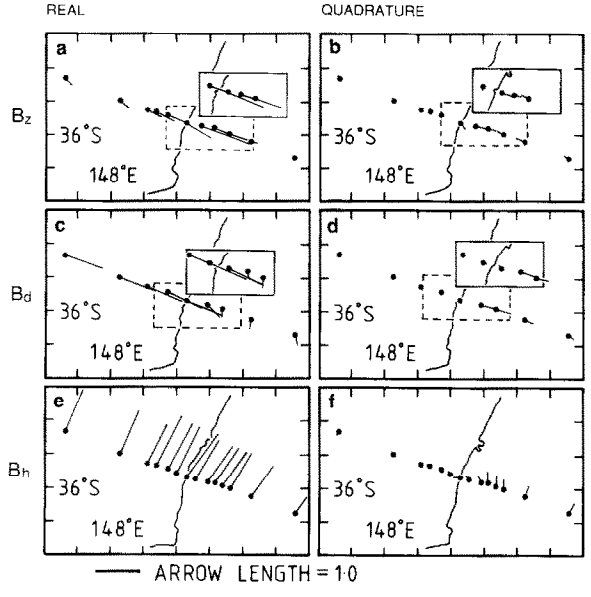

Fig. 2. Induction arrows for a period band centred on 7484 s (2.08 hr). Real arrows are shown on the left (a,c and e) and quadrature arrows on the right (b, d and f). The upper pair (a and b) are arrows for the local vertical magnetic field fluctuation, B_z, which corresponds to a horizontal field fluctuation of amplitude 1 nT at inland site GNS. The central pair (c and d) are for B_d arrows, computed as described in the text. The lower pair (e and f) are for B_h arrows. In the upper four figures some arrows are plotted in offset boxes for the sake of clarity. The correct position for the solid-line box is that of the dashed-line box.

The arrows have been determined by performing a least-squares minimisation of the misfit term in the standard equations. For the vertical field arrows the transfer function equation is:

$$B_z^a = T_{zh}B_h^n + T_{zd}B_d^n \quad (1)$$

and for the horizontal field arrows the equations are:

$$B_h^a = T_{hh}B_h^n + T_{hd}B_d^n \quad (2)$$

$$B_d^a = T_{dh}B_h^n + T_{dd}B_d^n \quad (3)$$

Here all parameters are taken to be functions of frequency. The geomagnetic north, east and vertically downwards components of magnetic fluctuation are denoted B_h, B_d and B_z, with superscripts "a" and "n" representing "anomalous" and "normal" respectively.

Taking real and quadrature parts separately, the vertical field transfer functions T_{zh} and T_{zd} generate the vertical field arrows shown in Figs. 2a and 2b: an arrow is formed with components T_{zh} and T_{zd} to the south and west respectively for the real part, and to the north and east respectively for the quadrature part. The "reversal" in plotting the real parts is to follow Parkinson's convention, so that a land arrow will generally point towards the higher side of a nearby electrical conductivity contrast (though note that the situation for seafloor recordings may be quite different).

To present the transfer functions T_{hh}, T_{hd}, T_{dh} and T_{dd} for the horizontal magnetic field fluctuations, a different procedure is followed: arrows are formed by calculating at each site the (total) response in the horizontal field to a real event of 1 nT occurring at the inland reference station GNS. Arrows denoted B_d in Figs. 2c and 2d are then given when the event at GNS is polarised parallel to the line of observing sites, and directed west to east. Arrows denoted B_h in Figs. 2e and 2f are given when the event at GNS is polarized perpendicular to the line of observing sites, and directed south to north. This technique is an exten-

sion of the hypothetical event analysis of Bailey et al. (1974), with the two particular polarisations at the inland reference station chosen to test the two-dimensional nature of the region. For the Tasman Experiment data, entire time series (of lengths up to 120 days) have been used in the transfer function computations to reduce bias which could result from analysing individual events (Kellett, 1989). The period bands chosen for arrow computation lie in the range 600 s to 180,000 s, and are determined by the sampling rate of the instruments, the shielding effect of the ocean layer, and the lengths of the time series. Spectral bands affected by tidal oceanic signals have been removed prior to band-averaging (Chave et al., 1981).

3.2. *Main features of the arrow patterns*

The strongest feature of Fig. 2 is the alignment of the vertical field arrows perpendicular to the coastline. This characteristic is especially clear in the real part (Fig. 2a), where it represents the traditional geomagnetic "coast effect". In Fig. 2c the arrow pattern is uniform across the continent, but there is a strong attenuation with depth in the seawater. On the seafloor the B_d arrow pattern is deflected to the south; also there is a shift in phase from real to quadrature, as the field diffuses down through the ocean. In Fig. 2e the arrow pattern similarly is approximately constant on the continent, but changes with depth in the ocean. The continent to seafloor contrast in the B_h arrow pattern is not as strong as for the B_d arrow pattern, due as shall be seen below to the contrast of the B-pol and E-pol cases, which B_h and B_d represent.

The strongly 2-D nature of the arrows in Fig. 2 gives confidence in a 2-D interpretation, and encourages the production of "pseudosections", as presented in Fig. 3. These pseudosections give the arrow results over a range of frequencies in the following manner.

First, a "real" fluctuation in the horizontal field of amplitude 10 nT is considered to occur at reference site GNS, directed west to east along the profile direction. Figures 3a and 3b present the real and quadrature amplitudes of the resulting vertical field fluctuation B_z at different geographic positions along the profile (horizontal axis), and for different periods of the phenomenon (vertical axis). Figures 3c and 3d similarly present the real and quadrature amplitudes of the component (denoted B_y) of the resulting horizontal field fluctuation which is directed along the direction of the profile (west to east).

Figures 3e and 3f takes the horizontal fluctuation at GNS to be directed parallel to the coastline, south to north, and presents the amplitude of the component (denoted B_x) of the resultant horizontal field fluctuation which is also parallel to the coastline, (or perpendicular to the profile). The pseudosections for B_y and B_x in Fig. 3 thus idealise the data as two-dimensional; in Fig. 2 the B_d and B_h arrows could in principle take any direction; but the B_y and B_x values in Fig. 3 are always for components parallel and perpendicular, respectively, to the profile.

Figures 3g and 3h present data for E_x determined by multiplying the appropriate component of an observed seafloor magnetotelluric impedance tensor (Ferguson, 1988; Ferguson et al., 1990) by the corresponding B_y value in Figs. 3c and 3d. Thus these values for E_x also correspond to a 10 nT horizontal fluctuation at GNS (directed along the profile, west to east). Similarly, the E_y values in Figs. 3i and 3j are determined from seafloor impedance tensors and the B_x values in Figs. 3e and 3f, and correspond to a 10 nT horizontal fluctuation at GNS (directed perpendicular to the profile, south to north).

The vertical span of the pseudosections is over fifteen period bands, spaced evenly on a logarithmic scale. Producing the pseudosections involved interpolating the data onto meshes of regularly spaced nodes, which were then contoured.

The B_z pseudosections show that the pattern of induction demonstrated by the arrows in Figs. 2a and 2b holds for all periods up to 50,000 s. Other important characteristics are the narrow width of the B_z anomaly at periods of about 1000 s across the continental shelf, and the reversal there of the quadrature part. With period increasing to 10,000 s, the quadrature part decreases while the real part reaches a second maximum. At periods greater than 10,000 s, the real part exhibits a broad

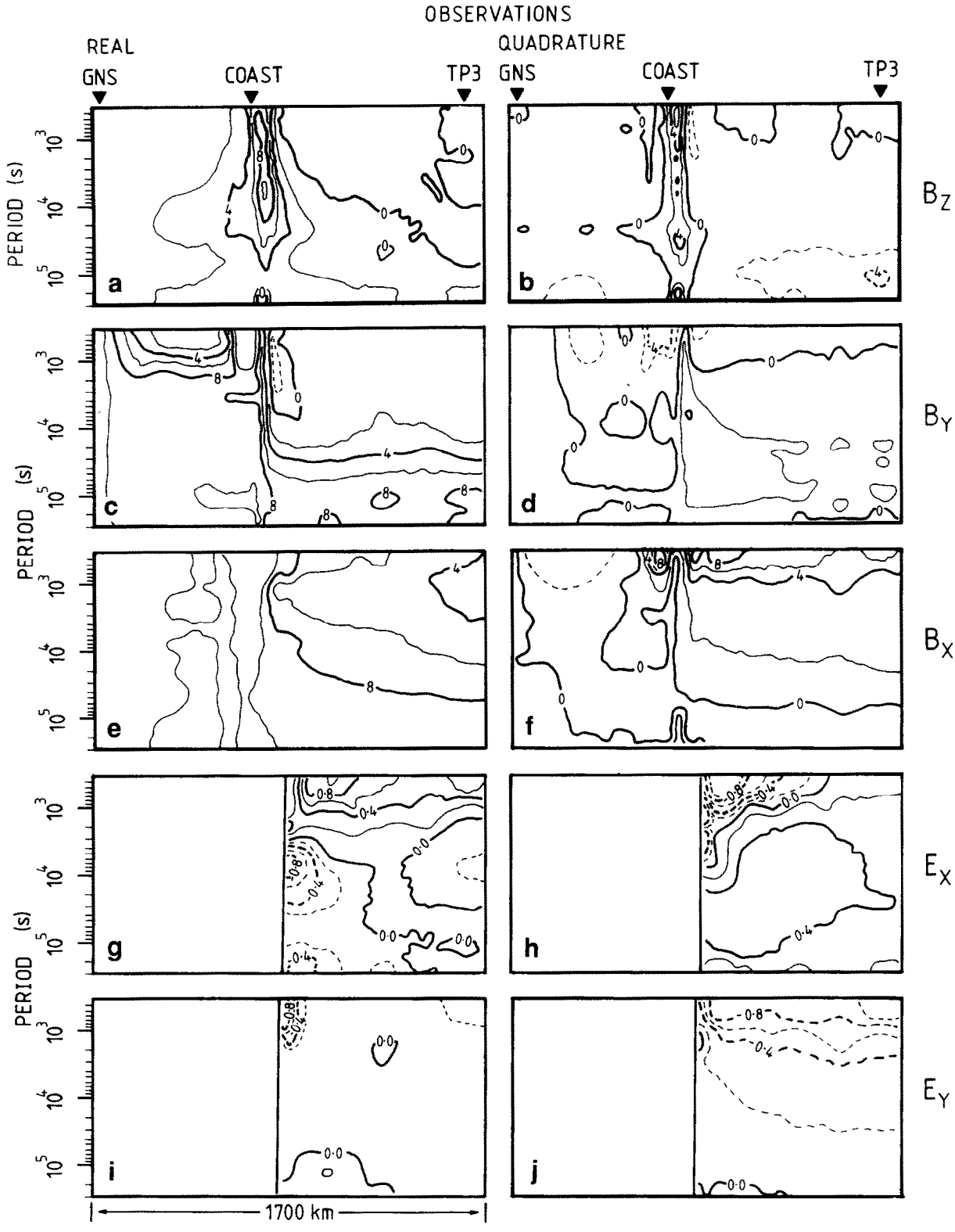

Fig. 3. Pseudosections of the observed magnetic and electric fields. The source field is an hypothetical event of 10 nT at site GNS. The data shown come from both land and seafloor sites between GNS and TP3 (a distance of 1500 km) on the Tasman profile (horizontal axis), and extend from 600 s to 170,000 s in fifteen logarithmically-spaced period bands (vertical axis). A source field polarised along the profile produces B_z (parts a,b), B_y (parts c, d) and E_x (parts g, h). A source field polarised perpendicular to the profile produces B_x (parts e, f) and E_y (parts i, j). The magnetic and electric field data are contoured at intervals of 2 nT and 0.2 μV m^{-1} respectively. Dashed contours represent negative values.

anomaly, which is abruptly lost at 40,000 s; the quadrature part is very small over a small period range centred at 30,000 s.

These characteristics of the B_z component can be compared with the results of previous studies. For example, DeLaurier et al. (1983) found that at short periods the quadrature part did reverse over the continental shelf of British Columbia, whereas Ogawa et al. (1986) found no evidence for a reversal at period 900 s on the continental shelf of Japan. Also, the persistence of the strong anomaly in the real part of B_z over the middle of the southeast Australian continental slope, even at long periods, contrasts with the results observed by the EMSLAB group (1988) for Pacific North America, where the maximum B_z value moved to deeper water at longer periods. These differences may well reflect the different tectonic settings of the respective coastlines.

Distinctive characteristics are also evident in the B_y pseudosections in Figs. 3c and 3d. The most notable is the simple attenuation with depth in the ocean. This attenuation is independent of period up to about 30,000 s, and at greater periods it is essentially absent. Corresponding to the phase shift of the field diffusing down through the ocean, the quadrature part is amplified immediately offshore, over a region which increases in width with increasing period.

The B_x sections in Figs. 3e and 3f show similar patterns to those of B_y in Figs. 3c and 3d except that the attenuation of the real part of B_x with depth in the ocean water, near the coast, is not as severe. This characteristic is consistent with the contrast of the E-pol and B-pol modes of 2-D induction.

4. Seafloor electric fields

A major achievement of the Tasman Experiment has been the observation of seafloor electric fields simultaneous with magnetic measurements. The patterns in Figs. 3g–j show that the spatial variation of electric fields at the floor of the Tasman Sea is smooth, with "coast effects" present (especially in E_x). With increasing period there is attenuation of both E_x and E_y at the seafloor.

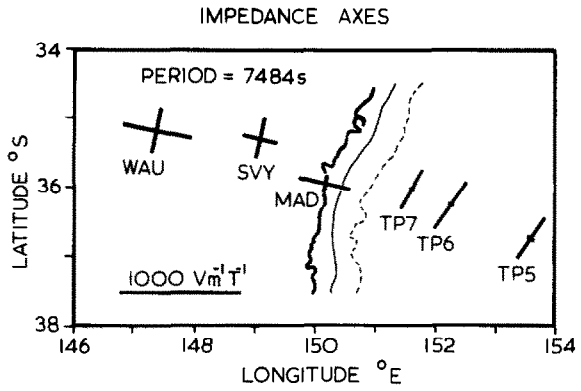

Fig. 4. Magnetotelluric impedance axes for land sites WAU, SVY and MAD (after Tammemagi and Lilley, 1971) and seafloor sites TP7, TP6 and TP5 (after Ferguson et al., 1990), for period 7484 s.

Figure 4 shows magnetotelluric impedances from Ferguson (1988) for the three most inshore Tasman sites, plotted with land magnetotelluric results from Tammemagi and Lilley (1971). The marine data show a consistent and simple pattern, as observed by Ferguson. The land data are from an earlier period, and are not of the same quality; nevertheless in Fig. 4 they are a valuable complement to the seafloor results.

The high degree of anisotropy in the marine data is attributed by Ferguson (1988), Lilley et al. (1989) and Ferguson et al., (1990) to the effect of the ocean–continent boundary. The land impedance tensors show less uniform behaviour (due possibly to the more complicated nature of continental geology), however a pattern of anisotropy is present. This land anisotropy was interpreted by Tammemagi (1972) as an illustration of the effect of the ocean–continent boundary, observed on the land side. Juxtaposition of the newer seafloor results with the earlier (if less accurate) land results reinforces this interpretation.

5. Inversion of the data

5.1 Strategy of modelling

The set of data described above is now inverted as a two-dimensional coast model. The basis of the inversion is "forward model" calculation, using the algorithms of Brewitt-Taylor and Weaver (1976), with confirmatory calculations using the

algorithms of Wannamaker et al. (1987). The parameter of misfit used for model choice is described in section 5.2 below. The best model is taken to be that of minimum misfit.

The modelling procedure is one of systematic search through a range of models, and is designed to test for contrasts in the electrical conductivity structure across the continent-ocean boundary, in addition to the seawater-land contrast. The range of the search is intended to be wide enough to seek a "global" minimum of misfit, and so to avoid the hazard of being led into a local minimum. The scope of the search is limited by the size of the computing task involved, and for simplicity only conductivity profiles which increase with depth are considered. The modelling procedure has been found to be insensitive to steps in a profile where conductivity decreases with depth.

5.2 *Parameter of misfit*

The misfit parameter chosen is based on the common weighted least-squares misfit or L_2 norm:

$$\chi^2 = \sum_{i=1}^{N} \left[W_i (D_i - M_i) \right]^2 \tag{4}$$

where D_i is an observed datum, M_i is a model response, W_i is the weight and N is the number of observations available.

For such a misfit, it is important to set some criteria for acceptance or rejection of a particular model; that is, to set a tolerance. Parker (1983), after considering the concept of a "satisfactory model", took Gaussian statistics and a χ^2 measure of misfit, and set the tolerance to be two standard deviations of χ^2 greater than the expected value. Thus (see also Parker and Whaler, 1981):

$$N < \chi^2 < N + 2(2N)^{\frac{1}{2}} \tag{5}$$

where N is the number of independent data. A model response with a misfit smaller than the expected value passes within the uncertainty bars on the observed data, and contains information which the data cannot resolve; hence N is usually adopted as the lower bound on the tolerance.

5.3. *Applying a measure of misfit*

The misfit of a model in this paper is based on as large a number of independent observations as possible ($N = 372$), from a data set of the real and quadrature parts of B_z, B_y, B_x, E_x and E_y at three periods from the Tasman and Continental Slope experiment sites. The actual measure taken is the root-mean-square (RMS) misfit, here denoted R, given by:

$$R = \sqrt{\frac{1}{N} \sum_{i=1}^{N} \left[\frac{D_i - M_i}{\delta D_i} \right]^2} \tag{6}$$

This misfit parameter, subject to uncertainties (δD_i) in the observed data, places equal weight on all response functions. The effect of such weighting is difficult to assess, however it is clear that the concentration of sites close to the coast will cause a greater emphasis on the fit of the model beneath that part of the profile. The periods chosen are evenly distributed on a logarithmic scale so there should be no particular bias towards either shallow or deep structure. For the RMS misfit the tolerance levels are given by:

$$1 < R < 1 + \left(\frac{2}{N} \right)^{\frac{1}{2}} \tag{7}$$

5.4. *Search and results*

The basic model of the search comprises, at the surface, an ocean adjoining a continent. The ocean has the known bathymetry of the Tasman Sea, and its boundary with the land is a cross section of the known continental slope and shelf. The seawater has an electric conductivity of 3.3 S m^{-1}, and immediately beneath the deep ocean floor is a layer of conductivity 1.0 S m^{-1} and thickness 1.0 km, representing the known sediment on the Tasman Abyssal Plain.

The deeper structure is divided into two distinct regions, continental and oceanic, with the vertical boundary between them placed beneath the edge of the continental shelf. For the first part of the search the continental conductivity profile, typical of a non-shield distribution and based on the results and discussions of Tammemagi and

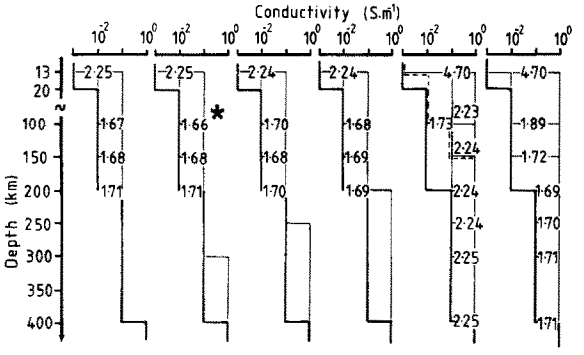

Fig. 5. Electric conductivity profiles and results of the systematic search described in the text. The thick solid line represents the continental profile taken as standard. The thin lines give the oceanic profiles searched. The RMS misfit for each model is placed at the position corresponding to its first increase of conductivity with depth. Moving from left to right across the figure corresponds to a shallowing of a second conductivity increase. The asterisk indicates the minimum misfit.

Lilley (1971), Lilley et al. (1981), and Parkinson and Hutton (1989) is fixed and the oceanic conductivity profile, below the abyssal plain sediments, is varied. The range of the search thus carried out is shown in Fig. 5. The RMS misfit determined for the various models of the search is also tabulated in Fig. 5, and the minimum value is marked with an asterisk.

A further part of the search involved varying the continental profile, with the oceanic profile fixed at the best-fitting profile found above. This procedure produced no further reduction in misfit, as neither did a systematic search of oceanic profiles against a continental shield profile (which was of lower conductivity at each depth down to 400 km than the standard shown in Fig. 5). Also, moving the vertical boundary between continental and oceanic profiles a horizontal distance of up to 100 km on either side of the continental shelf produced no further reduction in misfit.

The model marked with an asterisk in Fig. 5 is thus the best-fitting model. This model is shown in Fig. 6, and its computed responses are shown in Fig. 7 as pseudosections, for direct comparison with the observed pseudosections of Fig. 3. The pseudosections contain much information, and comparison of Fig. 7 with Fig. 3 gives a visual impression of the fit of the model to the data. To illustrate the fit another way, Fig. 8 shows traditional profiles of the model response at one particular period, with the appropriate observed data. The excellence of the fit of the magnetic data (reminiscent of the model in White et al. 1990, which essentially was a "seawater only" model) is well displayed. For the electric field data, E_y fits well, and E_x less so: though the figure shows the E_x misfit to be perhaps in phase rather than in amplitude.

Given the modelling scheme developed in this study, it is difficult to obtain a quantitative estimate of the uncertainty in the depth of the boundaries shown in Fig. 6. The R value for the preferred model in Fig. 5 is 1.66, which exceeds the upper tolerance value of 1.07 derived from eqn. 7. While adding fine structure to the conductivity model in Fig. 6 might reduce this misfit further, it is considered likely that the misfit mainly reflects departures of the actual induction process from the ideal two-dimensional case of the model. These departures further complicate any assessment of the errors in the depths of the conductive layers. Qualitatively this study indicates that even though the continental structure of Fig. 6 is less well constrained than the oceanic structure, the good conductor at 200 km cannot be moved up to 100 km without substantially increasing the misfit. On the oceanic side of Fig. 6, the good conductor shown at 100 km depth must be shallower than 200 km and cannot be placed immediately below the crust.

Tests of the sensitivity of the misfit parameter to changes in the oceanic structure demonstrate an important lesson of the present modelling ex-

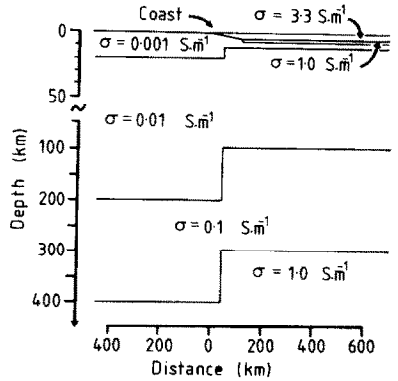

Fig. 6. Cross section of the best-fitting two-dimensional model.

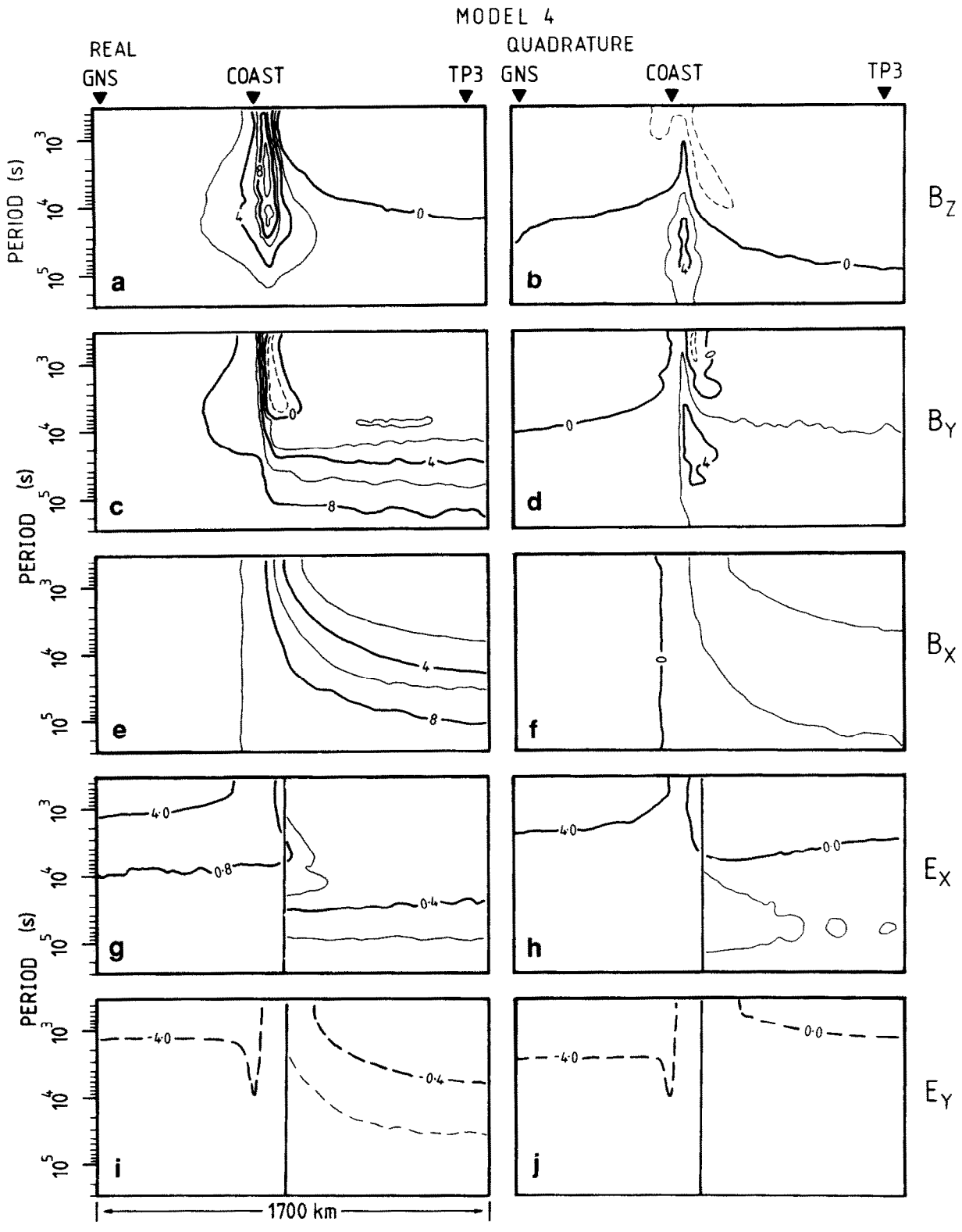

Fig. 7. Pseudosections of the calculated magnetic and electric fields for the best-fitting model (shown in Fig. 6). The source field is an hypothetical event of amplitude 10 nT at the left-hand surface of the model; all other details are as for Fig. 3. Only major contours are shown on the left-hand sides of the lower two pairs of diagrams.

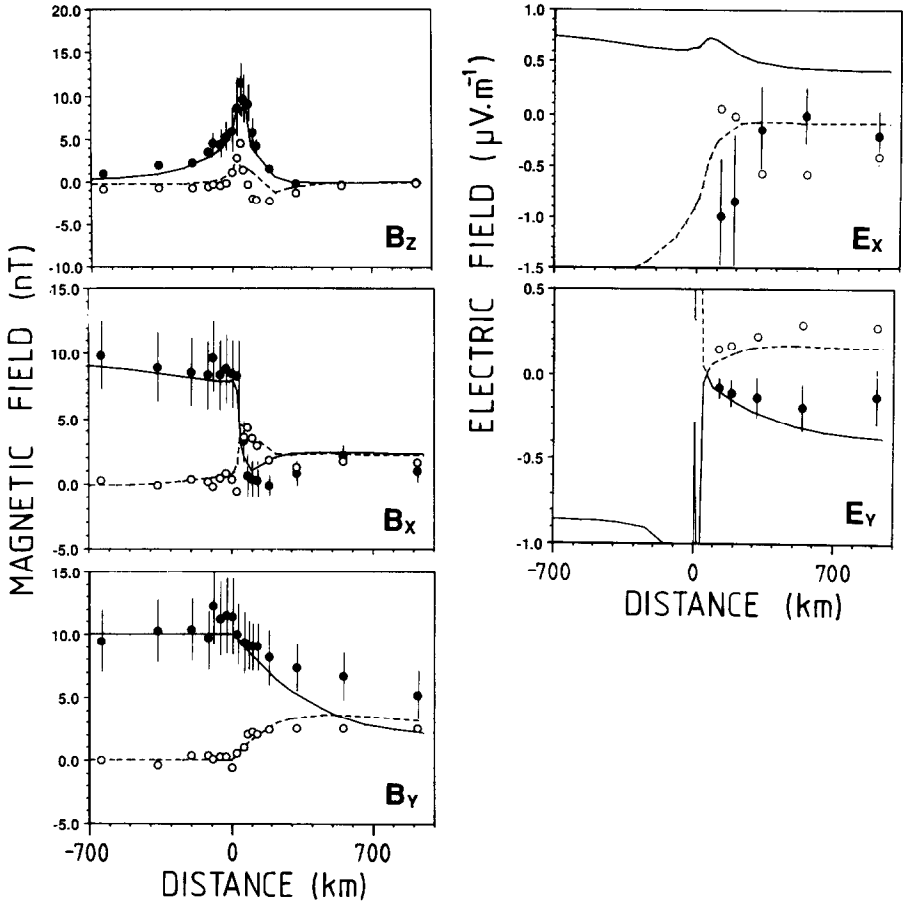

Fig. 8. Profiles of the magnetic and electric fields computed for the best-fitting model, shown as continuous lines for the real parts, and dashed lines for the quadrature parts. Observed data are plotted as solid points for real, open points for quadrature. Error bars for the quadrature points are similar to those of the real points, and are not plotted in the interests of diagram clarity. The quadrature parts of the electric fields have been plotted with reversed signs, to prevent them from being obscured by the real parts. All information for period 7484 s.

ercise: that generally it is the seafloor electric field data which provide the most demanding criteria for determining the depth of the good conductor and establishing a change in its depth across the continent-ocean boundary (Kellett, 1989). The improvement in model misfit from that of a seawater-only model of White et al. (1990), made possible by the inclusion of the seafloor electric field data, is significant.

6. Seismic evidence

There is evidence, from seismological studies, of shear waves in the depth range 200 to 400 km being significantly slower under oceanic basins than under continental shields (Grand and Helmberger, 1984). In the Tasman Sea region, a study of the travel time residuals for the S, P, ScS and ScP seismic phases from earthquakes in the Tonga Benioff zone showed a systematic change from large positive residuals at oceanic stations to much smaller residuals (negative for S–P) at stations in central Australia. This dependence of the residual on the tectonic setting of the receiver suggested that the shear velocity in the top 400 km of the mantle beneath the Tasman Sea was up to 4% slower than under central Australia (Frohlich and Barazangi, 1980).

More detailed modelling of the shear wave velocities in the top 220 km was performed by Sundaralingam and Denham (1987). They inverted the group and phase velocities of Rayleigh

waves for paths crossing the Tasman and Coral sea regions. Of particular interest are the one dimensional velocity models of the East Australian continent, the Tasman basin and the Lord Howe Rise. The study concentrated on determining the thickness and velocity of the lithospheric "lid" and the velocity of the underlying layer. The Tasman basin section consisted of a lid which extended from the base of the thin oceanic crust down to a depth of 75 km, and had a marked drop in velocity at its base. The Lord Howe Rise profile had a similar lid except it extended to a depth of 85 km. The East Australian profiles showed a much smaller velocity decrease at a depth of 90 km.

Global tomography, using seismic shear waves, also indicates a contrast at upper mantle depths between the material beneath continental Australia and the material beneath the Tasman Sea. The results of Woodhouse and Dziewonski (1984) show that at depth 300 km the shear velocity may be several percent slower under the Tasman Sea than under the continent region, and a difference is still perceptible at depth 550 km. The contrast is interpreted as indicating warmer oceanic mantle, and the figures of Woodhouse and Dziewonski (1984) show, within their own resolution, a boundary in seismic shear velocity which follows quite closely the continental shelf of southeast Australia. There is thus support from seismic evidence for a model such as that of Fig. 6, with contrasts in structure at depth.

7. Interpretation

7.1. Tectonic setting

The model of Fig. 6 is not, in its main characteristics, different from previous models of the coast effect; neither generally nor, indeed, for southeast Australia in particular: compare fig. 7 of Bennett and Lilley (1974). However, Fig. 6 represents modelling with a degree of control which has not been possible before. The interpretation of Fig. 6 may thus be linked to previous coast-effect interpretations, and a relatively straightforward interpretation is possible in terms of the formation of the southeast Australian continental shelf by the opening of the Tasman Sea.

The southeast Australian continental margin is one of many margins which formed during the Late Mesozoic breakup of Gondwana. For southeast Australia the timing and pattern of the fragmentation is poorly constrained, because most of the blocks involved have either undergone major subsequent episodes of deformation, or are now submerged beneath sea or ice.

Nevertheless, the pattern of seafloor magnetic anomalies and fracture zones in the Tasman Basin shows that the process of seafloor spreading was complex. The oldest seafloor adjacent to east Australia has been inferred from the magnetic anomaly time scale and the observed sedimentary cover to be approximately 75 Ma, and the youngest anomaly in the centre of the Tasman Sea gives an age of 53 Ma for the end of spreading (McDougall and Duncan, 1988). The major fracture zones which cut the spreading ridge can be correlated with tectonic features within continental east Australia, supporting the evidence that existing crustal features played an important role in the early stages of spreading (Ringis, 1975). Spreading rates probably varied considerably across the major transforms, and through time, however the south Tasman Sea had a fast average spreading rate (Weissel and Hayes, 1977; Shaw, 1978).

The extreme asymmetry in the bathymetry and sedimentary record across the conjugate margins of the Tasman Sea and the Lord Howe Rise has been discussed by Jongsma and Mutter (1978). They proposed that the rifting began symmetrically but that after a period of extension the locus of rifting jumped to the western edge of the rift valley. Seafloor spreading began immediately adjacent to the unextended east Australian flank, and the entire rift valley sequence was carried with the Lord Howe Rise. Lister et al. (1990) considered the two margins to be type examples of the lithosphere detachment model for Atlantic-type margin formation. Southeast Australia is the "upper plate" margin, with an uplifted rift flank and basaltic underplating whilst the Lord Howe Rise is a highly extended continental block on the "lower plate". These authors include the Norfolk

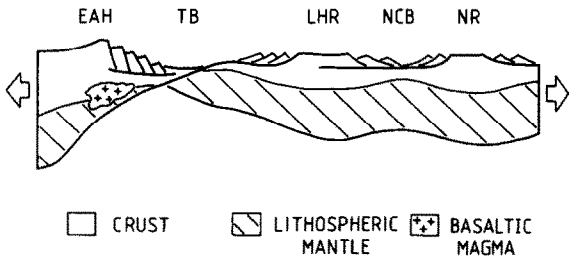

Fig. 9. A lithosphere detachment model for the structure of the southeast Australian continental margin. *EAH* = East Australian Highlands, *TB* = Tasman Basin, *LHR* = Lord Howe Rise, *NCB* = New Caledonia Basin, *NR* = Norfolk Ridge.

Ridge and New Caledonia Basin in the lower plate, emphasising the large amount of extension that can occur in the lower plate. The model of Lister et al. (1991) is shown in Fig. 9.

In summary, the present information about the rifting episode between the Lord Howe Rise and east Australia suggests that it was in response to a regional horizontal stress field rather than in response to an active source of mantle upwelling below east Australia. The region of rifted continental material may have been very wide with the focus of extension shifting several times and the final breakup occurring adjacent to the relatively unextended east Australia.

7.2. Post seafloor-spreading history

During the 53 M.y. since the end of seafloor spreading, the Tasman Sea region has remained fixed to the Australian plate. However, the southern part of the Lord Howe Rise has continued to move relative to the Australian continent, as the continental blocks of New Zealand have accommodated the establishment of a new Pacific/Indo-Australian plate boundary. The present depths below sea level of the basaltic basement in the Tasman Basin, and the present heatflow (Grim, 1967) are consistent with the predictions based on a model in which the oceanic lithosphere cools and thickens as it moves away from the spreading centre, and gets older (Parsons and Sclater, 1977).

The whole Indo-Australian plate has moved northwards relative to the Antarctic plate over the last 24 M.y., and this motion has been recorded by the Tasmantid Seamount chain, the Lord Howe Seamount chain and the volcanic activity in east Australia (McDougall and Duncan, 1988). The amount of heat associated with these hotspots has not been sufficient to produce a large Hawaiian type swell, and has probably only perturbed the lithosphere immediately beneath the site of volcanism. Thus despite the narrow continental shelf and the absence of major sedimentary basins, the southeast Australian continental margin appears to be a boundary between a region of typical Palaeozoic continental lithosphere and typical Late Mesozoic oceanic lithosphere.

7.3. The electric conductivity changes during passive (or "Atlantic-type") margin formation

The electric conductivity model produced for southeast Australia is thus consistent with other geophysical features. It is a structure which has developed over the 100 M.y. or so since rifting began. The part of the Wilson Cycle involving continental rifting and seafloor spreading has been studied in great detail from the point of view of the thermal and mechanical changes in the lithosphere, and it is of some interest to consider here the corresponding changes in electric conductivity.

A model is thus shown in Fig. 10 for the development of the conductivity structure deduced to exist beneath eastern Australia and the Tasman Sea. The main features of this model may well be general for such passive (or "Atlantic-type") continental margins. The model is constrained to produce, in a general way, the main features of Fig. 9 above.

In Fig. 10 the electric conductivity is indicated by profiles for sites *A* and *B*, and the heavy dashed line which marks the top of a conductivity increase.

The model has five stages:

(1) The conductivity structure is that of a Palaeozoic fold belt with a thickened crust (40 km) of 10^{-3} S m^{-1}, a lower lithosphere (100 km) of 10^{-2} S m^{-1} and a conductivity increase at 200 km depth.

(2) The region is subjected to extensional stresses which thin the crust by faulting and block rotation. The lower lithosphere thins in a ductile manner and the asthenosphere rises to replace the

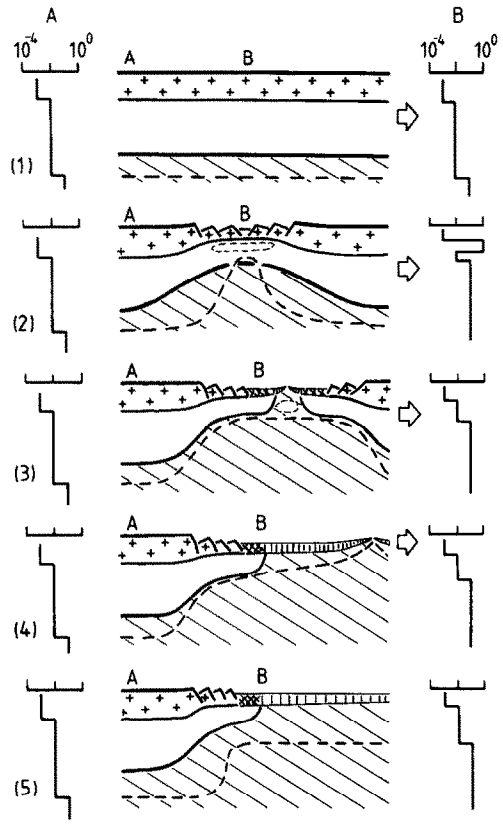

Fig. 10. A model for the development of the electric conductivity structure at the continental margin of southeast Australia, as a type-example for passive or "Atlantic-type" continental margins generally. The top panel is typical lithosphere and asthenosphere prior to extension, and the bottom panel is the continental margin some 100 M.y. later. Continental crust is marked by plus signs, lithospheric mantle is unmarked, asthenosphere is marked by diagonal lines, oceanic crust is marked by vertical lines, and transitional crust is marked by cross-hatching. The conductivity structure is shown as conductivity profiles (in units of S m^{-1}) below site *A* (shown left) and site *B* (shown right). The heavy and light dashed lines mark conductivity boundaries: below the heavy dashed line the conductivity is 0.1 S m^{-1}; within the light dashed contours the conductivity exceeds 1.0 S m^{-1} (as partial melt).

lost material. The conductivity structure at site A is unperturbed but at site B the structure is typical of that seen in modern continental rifts such as the Rio Grande, Baikal and East African rifts, and the Rhine Graben. A good conductor is seen at depths of 20 to 30 km associated with fluids or a zone of melt accumulation (Hermance, 1982). Deeper studies under the western U.S. suggest that a zone of high conductivity exists between 50 and 200 km (Gough, 1974).

(3) The crust has thinned from 40 km to 10 km by faulting and large volumes of magma have been extruded at the centre of the rift, producing a hybrid continental–oceanic crust. (The modern spreading centre in Iceland may be a good analogue, despite its anomalous position over a large hotspot.) The crust is 15 km thick and the Moho is underlain by a zone of high conductivity (Beblo and Bjornsson, 1980). Between 50 and 150 km the conductivity is uniformly high representing a region of low geothermal gradient but elevated temperatures, producing a moderate conductivity. For this stage a representative tectonic regime may be the northern Gulf of California, where the Pacific Plate margin changes from a transcurrent fault to a set of offset spreading centres. For this area White (1973) demonstrated the presence of a good conductor in a narrow zone, which may come to within 30 km of the surface.

(4) As seafloor spreading progresses, site *B* moves away from the region of melt generation, and the lithosphere beneath the site begins to cool and thicken. The elastic lithosphere relaxes and isostatic equilibrium is restored. The good conductor begins to subside in advance of the newly forming lithosphere. Under ocean basins the conductivity increase descends at a rate of about 1 km/M.y.

(5) Some 100 M.y. after Stage (3), the conductivity increase beneath the ocean basin has moved down to 100 km depth; under the continent, it has returned to its pre-rift 200 km depth. In southeast Australia the zone of transition between the two regions may be very narrow, due to the absence of any extended continental margin. Throughout this process, the deeper conductive layer will also be perturbed beneath the oceanic region, and may take significantly longer to return to some equilibrium.

8. Conclusions

The conclusion of the work described in this paper is that the geomagnetic coast-effect in southeast Australia and the Tasman Sea can be explained to first order by the induction of electric current in the oceans. Two-dimensional models which include Tasman Sea bathymetry, seafloor

sediment and a one-dimensional crust and mantle produce most of the features resolved in the pseudosections of the magnetic fields B_x, B_y and B_z. The seafloor electric field data E_x and E_y provide extra model-fitting criteria, and the full set of data are best fitted by a model which includes a conductivity contrast between continent and ocean over the depth range 100 to 200 km. In addition to this major contrast, the modelling results also suggest contrasts within the depth ranges 13–20 km and 300–400 km.

The final model has an RMS misfit of 1.66 which is still outside the two standard deviation tolerance limit. The misfit is concentrated in the electric field component parallel to the continental margin (E_x) and cannot be isolated to any particular period. Various aspects of the data suggest that significant three-dimensional effects may prevent a better-fitting model from being found.

Keeping in mind all the approximations made when modelling is carried out in two dimensions, the conductivity structure proposed for the southeast Australian continental margin is consistent with other geophysical evidence. To some extent southeast Australia is a typical Atlantic-type margin, and the five-stage model illustrating its development can be considered appropriate for many other parts of the world. Using such a conceptual model, the variation in the depth to the asthenosphere across a margin can be estimated, taking into account the specific history of that margin. The following factors are concluded to be of major importance in determining the present electrical conductivity structure across a coastline, and the ability to resolve that structure given the dominating effect of the ocean.

(1) The age and previous tectonic history of the continental region which is being rifted will affect the distribution of electrical conductivity anomalies within the lithosphere, and may also play an important role in controlling the location and style of final break up.

(2) The driving mechanism for the rifting will further influence both the shallow and deep structure. Active rifting produced by a hotspot will perturb the conductivity structure to a greater depth than passive rifting.

(3) The width of extended and thinned continental lithosphere preserved on the continental margin is important because it will determine the width of the zone of transition between the deep continental conductivity increase and the shallower oceanic conductive layer. It will also determine whether observing instruments can be located so as to resolve the transition.

(4) The length of time that has passed since rifting will determine to what extent the conductivity structure under the continent and the shelf has relaxed to its pre-rift state.

(5) The subsequent history of the coastline is important because activity such as the passage of the margin over a major hotspot, or a period of subduction or transcurrent faulting along the margin, may overprint the rifting signature.

Acknowledgements

We have benefitted from discussions with and help from many people in undertaking the work described. We especially acknowledge contributions from N.L. Bindoff, G.F. Davies, I.J. Ferguson, J.H. Filloux, G.S. Heinson and B.L.N. Kennett. J.T. Weaver and P. Wannamaker are thanked for supplying modelling codes. Merren Sloane helped greatly with data reduction and Brenton Perkins played a major role in the securing of the Continental Slope Experiment data; in this matter we also acknowledge the part played by the master and crew of the R.V. "Franklin". Valuable comments were made by two anonymous referees and they are thanked for adding to the final version of the paper. The Continental Slope Experiment was supported by the Australian Research Council and Flinders University Research Committee. During the work described, R.L.K. held a Research Scholarship at the Australian National University.

References

Bailey, R.C., Edwards, R.N., Garland, G.D., Kurtz, R. and Pitcher, D., 1974. Electrical conductivity studies over a tectonically active area in eastern Canada. J. Geomagn. Geoelectr., 26: 125–146.

Banks, R.J., 1986. The interpretation of the Northumberland Trough geomagnetic variation anomaly using two-dimen-

sional current models. Geophys. J. R. Astron. Soc., 87: 595–616.

Beblo, M. and Bjornsson, A., 1980. A model of electrical resistivity beneath Iceland, correlation with temperature. J. Geophys., 47: 184–190.

Bennett, D.J. and Lilley, F.E.M., 1971. The effect of the southeast coast of Australia on transient magnetic variations. Earth Planet. Sci. Lett., 12: 392–398.

Bennett, D.J. and Lilley, F.E.M., 1974. Electrical conductivity structure in the southeast Australian region. Geophys. J. R. Astron. Soc., 37: 191–206.

Bindoff, N.L., 1988. Electromagnetic Induction by Oceanic Sources in the Tasman Sea. PhD Thesis, Australian National University, Canberra.

Bindoff, N.L., Lilley, F.E.M. and Filloux, J.H., 1988. A separation of ionospheric and oceanic tidal components in magnetic fluctuation data. J. Geomagn. Geoelectr., 40: 1445–1467.

Brewitt-Taylor, C.R. and Weaver, J.T., 1976. On the finite difference solution of two-dimensional induction problems. Geophys. J. R. Astron. Soc., 47: 375–396.

Chave, A.D., Von Herzen, R.P., Poehls, K.A. and Cox, C.S., 1981. Electromagnetic induction fields in the deep ocean north-east of Hawaii: implications for mantle conductivity and source fields. Geophys. J. R. Astron. Soc., 66: 379–406.

DeLaurier, J.M., Auld, D.R. and Law, L.K., 1983. The geomagnetic response across the continental margin off Vancouver Island: comparison of results from numerical modelling and field data. J. Geomagn. Geoelectr., 35: 517–528.

EMSLAB group, 1988. The EMSLAB electromagnetic sounding experiment. Eos, Trans. Am. Geophys. Union, 69: 89–99.

Everett, J.E. and Hyndman, R.D., 1967. Geomagnetic variations and the electric conductivity structure of south-western Australia. Phys. Earth Planet. Inter., 1: 24–34.

Ferguson, I.J., 1988. The Tasman Project of Seafloor Magnetotelluric Exploration. PhD Thesis, Australian National University, Canberra.

Ferguson, I.J., Lilley, F.E.M. and Filloux, J.H., 1990. Geomagnetic induction in the Tasman Sea and electrical conductivity structure beneath the Tasman Seafloor. Geophys. J. Inter., 102: 299–312.

Filloux, J.H., 1988. Instrumentation and experimental methods for oceanic studies. In: J.A. Jacobs (Editor), Geomagnetism, Vol. 1. Academic Press, New York, pp. 143–247.

Frohlich, C. and Barazangi, M., 1980. A regional study of mantle variations beneath eastern Australia and the southwestern Pacific using short-period recordings of P, S, PcP, ScP and ScS waves produced by Tongan deep earthquakes. Phys. Earth. Planet. Inter., 21: 1–14.

Gough, D.I., 1974. Electrical conductivity under western North America in relation to heat flow seismology and structure. J. Geomagn. Geoelectr., 26: 105–112.

Grand, S.P. and Helmberger, D.V., 1984. Upper mantle shear structure beneath the northwest Atlantic ocean. J. Geophys. Res., 89: 11465–11475.

Grim, P.J., 1967. Heat flow in the Tasman Sea. J. Geophys. Res., 74: 3933–3934.

Heinson, G.S. and Lilley, F.E.M., 1989. Thin-sheet EM modelling of the Tasman Sea. Explor. Geophys., 20: 177–180.

Hermance, J.F., 1982. Magnetotelluric and geomagnetic deep sounding studies in rifts and adjacent areas: constraints on physical processes in the crust and upper mantle. In: G. Palmason, P. Mohr, K. Burke, R.W. Girdler, R.J. Bridwell and G.E. Sigvaldason (Editors), Continental and Oceanic Rifts. Am. Geophys. Union, Geodyn. Ser., 8: 169–192.

Jongsma, D. and Mutter, J.C., 1978. Non-axial breaching of a Rift valley: evidence from the Lord Howe Rise and southeast Australian margin. Earth Planet. Sci. Lett., 39: 226–234.

Kellett, R.L., 1989. Electric conductivity structure of the southeast Australian margin. PhD Thesis, Australian National University, Canberra.

Kellett, R.L., White, A., Ferguson, I.J. and Lilley, F.E.M., 1988. Geomagnetic fluctuation anomalies across the southeast Australian coast. Explor. Geophys., 19: 294–297.

Lilley, F.E.M., Woods, D.V. and Sloane, M.N., 1981. Electrical conductivity profiles and implications for the absence or presence of partial melting beneath central and southeast Australia. Phys. Earth Planet. Inter., 25: 419–428.

Lilley, F.E.M., Filloux, J.H., Ferguson, I.J., Bindoff, N.L. and Mulhearn, P.J., 1989. The Tasman Project of Seafloor Magnetotelluric Exploration: experiment and observations. Phys. Earth Planet. Inter., 53: 405–421.

Lister, G.S., Etheridge, M.A. and Symonds, P.A., 1991. Detachment models for the formation of passive continental margins. Tectonics, in press.

McDougall, I. and Duncan, R.A., 1988. Age progressive volcanism in the Tasmantid seamounts. Earth Planet. Sci. Lett., 89: 207–220.

Neumann, G.A. and Hermance, J.F., 1985. The geomagnetic coast effect in the Pacific Northwest of North America. Geophys. Res. Lett., 12: 502–505.

Ogawa, Y., Yukutake, T. and Utada, H., 1986. Two-dimensional modelling of resistivity structure beneath the Tohoku district, northern Honshu of Japan, by finite element method. J. Geomagn. Geoelectr., 38: 45–79.

Parker, R.L., 1983. The magnetotelluric inverse problem. Geophys. Surv., 6: 5–25.

Parker, R.L. and Whaler, K.A., 1981. Numerical methods for establishing solutions to the inverse problem of electromagnetic induction. J. Geophys. Res., 86: 9574–9584.

Parkinson, W.D., 1959. Directions of rapid geomagnetic fluctuations. Geophys. J. R. Astron. Soc., 2: 1–14.

Parkinson, W.D. and Hutton, V.R.S., 1989. The electrical conductivity of the Earth. In: J.A. Jacobs (Editor), Geomagnetism, Vol. 3. Academic Press, London, pp. 261–321.

Parkinson, W.D. and Jones, F.W., 1979. The geomagnetic coast effect. Rev. Geophys. Space Phys., 17: 1999–2015.

Parsons, B. and Sclater, J.G., 1977. An analysis of the variation of ocean floor bathymetry and heat flow with age. J. Geophys. Res., 82: 803–827.

Ringis, J., 1975. The relationship between structures on the

southeast Australian margin and in the Tasman Sea. Bull. Aust. Soc. Explor. Geophys., 6: 39–41.

Shaw, R.D., 1978. Seafloor spreading in the Tasman Sea: a Lord Howe Rise–eastern Australia reconstruction. Bull. Aust. Soc. Explor. Geophys., 6: 75–81.

Sundaralingam, K. and Denham, D., 1987. Structure of the upper mantle beneath the Coral and Tasman seas, as obtained from group and phase velocities of Rayleigh waves. N. Z. J. Geol. Geophys., 30: 329–341.

Tammemagi, H.Y., 1972. A Magnetotelluric Study in Southeastern Australia. PhD Thesis, Australian National University, Canberra.

Tammemagi, H.Y. and Lilley, F.E.M., 1971. Magnetotelluric studies across the Tasman geosyncline, Australia. Geophys. J. R. Astron. Soc., 22: 505–516.

Wannamaker, P.E., Stodt, J.A. and Rijo, L., 1987. PW2D finite element program for solution of magnetotelluric responses of two-dimensional Earth resistivity structure. Report of Earth Science Lab., University of Utah Research Institute.

Weissel, J.K. and Hayes, D.R., 1977. Evolution of the Tasman Sea reappraised. Earth Planet. Sci. Lett., 36: 77–84.

White, A., 1973. A geomagnetic variation anomaly across the northern Gulf of California. Geophys. J. R. Astron. Soc., 33: 1–25.

White, A. and Polatajko, O.W., 1978. The coast effect in geomagnetic variations in south Australia. J. Geomagn. Geoelectr., 30: 109–120.

White, A., Kellett, R.L. and Lilley, F.E.M., 1990. The continental slope experiment along the Tasman Project profile, southeast Australia. Phys. Earth Planet. Inter., 60: 147–154.

Woodhouse, J.H. and Dziewonski, A.M., 1984. Mapping the upper mantle: three-dimensional modelling of Earth structure by inversion of seismic waveforms. J. Geophys. Res., 89: 5953–5986.